https://dx.doi.org/10.22161/ijaers.711.14 ISSN: 2349-6495(P) | 2456-1908(O)

Comparative Study and Sensitivity Analysis in Simulation of Non-Darcy Flow in Shale Gas Reservoirs

Marcelo Luiz de Oliveira Pessanha[1], Rebeca Costa Dias do Rosário[1], Grazione de Souza[1] and Helio Pedro Amaral Souto[1]

[1]Departamento de Modelagem Computacional, Universidade do Estado do Rio de Janeiro, Rua Bonfim, 25, Vila Amélia, 28625-570 - Nova Friburgo, RJ, Brazil
Emails: mar.oliveirabreder@gmail.com, rebecacostadias@gmail.com, gsouza@iprj.uerj.br, helio@iprj.uerj.br

Received: 14 Oct 2020; Received in revised form: 10 Nov 2020; Accepted: 12 Nov 2020; Available online: 16 Nov 2020

Abstract *— In this work, we perform a comparative study of flow models and a sensitivity analysis concerning some parameters, considering the effects of slipping and gas adsorption in shale gas reservoirs, using numerical simulation. We use the Finite Difference Method, a linearization based on the Picard method, and the Conjugate Gradient method to obtain the reservoir and production well pressures. The results obtained demonstrate the importance of the effects of slipping and adsorption in the variation of pressure in a single-phase isothermal gas flow. Mainly because some parameters in the flow models, depending on their values, can act favoring (or disfavoring) the pressure drop.*

Keywords *— **Adsorption. Finite Difference Method. Natural gas. Reservoir simulation. Slipping flow.***

I. INTRODUCTION

For decades, the oil industry has followed a standard strategy in the context of hydrocarbon exploration/exploitation: the search for rock formations of interest, the location of the reservoir rocks, the identification of the mechanisms of imprisonment, and well drilling. These procedures had been used by geologists, geophysicists, and engineers, aiming mainly at the production of hydrocarbons via vertical wells in reservoirs formed, for example, by sandstones or carbonates.

However, in the past two decades, new concepts of exploitation have emerged. Rock formations that were previously less important, to the point of not being considered economically viable, are currently seen as potential reservoirs. Among unconventional sources, shale gas reservoirs are gaining more and more relevance on the world stage [8].

1.1. Natural gas

Natural gas is a homogeneous fluid with low viscosity and density. In a reservoir, natural gas can be classified as dry (it does not contain molecules heavy enough to form a liquid hydrocarbon under surface conditions), for example, when composed essentially of methane. Generally, natural gas (depending on the reservoir and its characteristics) contains methane, ethane, propane, butane, pentane, and hexane, but we can also find other heavier components in it. The non-hydrocarbon parcels, considered as impurities, include carbon dioxide, hydrogen sulfide, and nitrogen. The primary component is always methane, which may represent 70 to 98% of the total, followed by ethane (which may reach 10%).

Natural gas is the cleanest and richest source of hydrogen among hydrocarbons and has high efficiency in energy conversion. The current trend is for natural gas to become one of the most important fuels in the global economy [12] due to economic and environmental reasons [29, 31]. See Fig. 1 for the breakdown of the internal energy supply in Brazil for the year 2019 [13].

In terms of its use, natural gas can provide heating, generate electricity, and we can use it as fuel for motor vehicles or in the production of hydrogen [12]. According to Economides and Wood [12], the world reserves of natural gas have been increasing at an an-

https://dx.doi.org/10.22161/ijaers.711.14 ISSN: 2349-6495(P) | 2456-1908(O)

nual rate of about 5% since the seventies. The number of countries with known natural gas reserves has grown from 40, in 1960, to 85 in 2005.

1.2. Shale gas

Non-conventional reservoirs differ from conventional ones, for example, in that they have a very low permeability. Among the non-conventional reservoirs, we can mention the tight-gas sands (low permeability reservoirs), the coal bed methane (in which there is gas adhered to coal veins), and the shale gas (gas in shale-like rocks). The latter, the focus of this work, typically have extremely low permeabilities, in the range of 10^{-6} to 10^{-9} Darcy, low porosity, gas adsorbed on the solid, and the gas slips on the pore surfaces of the reservoir. Its formations are composed of sedimentary rocks, consisting of clay minerals such as illite, smectite, and kaolinite [8].

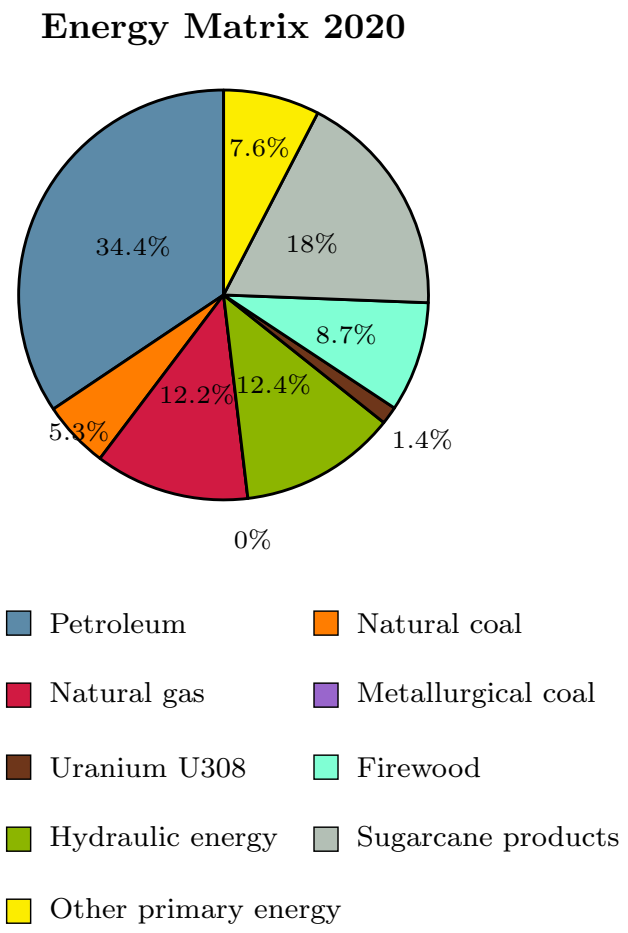

Fig. 1: *Supply by energy source in Brazil in 2019.*

In them, the gas is present as a free phase in the pores, dissolved in liquids, or adsorbed on solids. We find the gas adsorbed on carbon-rich compounds, such as kerogen. According to Ali [1], Wang [27] and Berawala [3], gas in an adsorbed state represents a fraction ranging from 20 to 80 % of the total gas reserves in shales. As the pressure decreases, as a result of continuous production, the gas adsorbed detaches from the solid and becomes part of the free phase, contributing to flow and production. Therefore, by neglecting the effects of adsorption, we can underestimate the potential of a shale reservoir [30].

About two decades ago, we considered gas recovery in shale reservoirs as economically and technically nonviable. However, with the emergence of new technologies, especially the drilling of horizontal wells and hydraulic fracturing, their exploitation has become possible and economically viable. In 2015, about three-quarters of natural gas production in the United States originated from these reservoirs, with the expectation of continued growth over the next two decades [28]. The great success in North America has led to unconventional sources gaining more attention on the world stage, including the countries of South America, such as Argentina and Brazil.

II. NATURAL GAS FLOW IN POROUS MEDIA

Typically, the classical Darcy law [7] is used in engineering to describe low-speed flows in porous media. For non-Darcy flows, it is modified and expressed in the form:

$$\mathbf{v} = -\frac{\mathbf{k}_a}{\mu}\left(\nabla p - \rho g \nabla D\right), \tag{1}$$

where $\mathbf{v}$ is the surface velocity of the fluid, $\mathbf{k}_a$ is the apparent permeability tensor, μ is the viscosity, p is the pressure, ρ is the density, g is the magnitude of the acceleration due to gravity, and D is the depth. Among the non-Darcy effects, which we can incorporate into the apparent permeability, we have:

- the inertial and turbulent effects,
- the non-Newtonian flow,
- the slipping and adsorption of the gas on the pore surface,

in addition to others that also cause non-linearity [2].

https://dx.doi.org/10.22161/ijaers.711.14 ISSN: 2349-6495(P) | 2456-1908(O)

2.1. The gas slippage phenomenon

Florence et al. [15] reported that the phenomenon of gas slipping occurs when the mean free path of the fluid molecules is of the order of the characteristic hydraulic radius of the pores. We know that gas flows in the porous medium differently from a liquid for two reasons: its high compressibility and the Klinkenberg effect [2]. We use Klinkenberg's correction to take into account the effects of gas slippage, which can be verified when carrying out permeability measurements on rock samples [14]

$$\mathbf{k_a} = \left(1 + \frac{b}{p}\right)\mathbf{k} \tag{2}$$

where b is the Klinkenberg parameter and $\mathbf{k}$ the absolute permeability tensor [19]. For example, gas slippage can occur in shale gas and tight gas sand reservoirs.

As an alternative to Klinkenberg's correction, we can also account for this effect through a more general expression for the determination of apparent permeability, which we can calculate as a function of Knudsen number [18],

$$\mathbf{k}_a = f(Kn)\mathbf{k} = (1 + \alpha_k Kn)\left(1 + \frac{4Kn}{1+Kn}\right)\mathbf{k}, \tag{3}$$

where $\mathbf{k}$ is the absolute permeability tensor, and α_k is the rarefaction parameter [18], whereas for the slip regime, $\alpha_k = 0$. The Knudsen number, Kn, is defined by

$$Kn = \frac{\lambda}{R_h}, \tag{4}$$

where λ is the average free path of the molecules and R_h the characteristic hydraulic radius [15]

$$R_h = 2\sqrt{2\tau}\sqrt{\frac{k}{\phi}} \tag{5}$$

and

$$\lambda = \frac{\mu}{p}\sqrt{\frac{\pi Z R T}{2M}}, \tag{6}$$

where τ is the tortuosity of the porous medium, k is the geometric mean representing the absolute permeability of the porous medium, ϕ the effective porosity of the porous medium, Z is the compressibility factor, T is the temperature, R is the universal constant for gases, M is the molecular mass of the gas, and $\gamma = M/M_{air}$ is the relative density of the gas and M_{air} the molecular mass of air [8]. The slip regime exists for the $10^{-3} < Kn < 0.1$ range [4].

2.2. The adsorption phenomenon

Adsorption occurs when the gas molecules attach to the solid surface of the pores, and the volume of gas adsorbed depends on the pressure of the gas phase. Here, we consider the Langmuir isotherm model:

$$V_{ads} = \frac{pV_L}{p + p_L}, \tag{7}$$

where V_{ads} is the volume of adsorbed gas, V_L is the maximum volume adsorbed (Langmuir volume), and p_L is the pressure corresponding to half of the maximum adsorption capacity (Langmuir pressure). According to Jiang and Younis [18], we can also incorporate the effects of adsorption into the calculation of apparent permeability

$$\mathbf{k'_a} = \left[1 - \frac{d_m}{R_h}\left(\frac{\frac{p}{p_L}}{1 + \frac{p}{p_L}}\right)\right]^4 \mathbf{k} \tag{8}$$

where d_m is the diameter of the gas molecule adhered to the surface. Therefore, we can combine the contributions due to gas slippage and adsorption in determining the apparent permeability in the form:

$$\mathbf{k}_a = f(Kn')\mathbf{k'}_a \tag{9}$$

where

$$f(Kn') = (1 + \alpha_k Kn')\left(\frac{1 + 4Kn'}{1 + Kn'}\right) \tag{10}$$

and the modified Knudsen number is set to

$$Kn' = \frac{\lambda}{R_{eff}}, \tag{11}$$

where

$$R_{eff} = R_h - d_m\left(\frac{\frac{p}{p_L}}{1 + \frac{p}{p_L}}\right) \tag{12}$$

https://dx.doi.org/10.22161/ijaers.711.14 ISSN: 2349-6495(P) | 2456-1908(O)

is the effective hydraulic radius.

2.3. Governing equation

According to Li et al. [21], the mass conservation equation, incorporating the effects of adsorption, is given by

$$\frac{\partial}{\partial t}\left(\frac{\rho_{sc}\phi}{B}\right)+\frac{\partial}{\partial t}\left(\frac{\rho_s\rho_{sc}V_{ads}}{B}\right)+\nabla\cdot\left(\frac{\rho_{sc}\mathbf{v}}{B}\right)$$

$$-\frac{q_{sc}\rho_{sc}}{V_b}=0, \tag{13}$$

where q_{sc} is a source term, ρ_s is the density of the rock, $B=\rho_{sc}/\rho$ is the volume formation factor, V_b is the total volume of the volume control (rock plus pores), and the subscript sc indicates the standard conditions,

$$\phi=\phi^0\left[1+c_\phi\left(p-p^0\right)\right], \tag{14}$$

where the superscript 0 indicates the reference conditions, and c_ϕ is the compressibility coefficient of the rock. We consider here small and constant rock compressibility.

Substituting Eq. (1) in Eq. (13) and considering that: ρ_{sc} and ρ_s are constant, we neglect the gravitational effects, the flow is two-dimensional, and the apparent permeability tensor is diagonal,

$$\frac{\partial}{\partial x}\left(\frac{k_{ax}}{\mu B}\frac{\partial p}{\partial x}\right)+\frac{\partial}{\partial y}\left(\frac{k_{ay}}{\mu B}\frac{\partial p}{\partial y}\right)-\frac{J_w}{V_b}\left(p-p_{wf}\right)$$

$$=\left(\Gamma'_p+\Gamma'_s\right)\frac{\partial p}{\partial t} \tag{15}$$

where for a non-isothermal flow and considering the previous expressions of V_{ads} and B

$$\Gamma'_p=\frac{c_\phi\phi^0}{B}+\phi\frac{d}{dp}\left(\frac{1}{B}\right) \tag{16}$$

and

$$\Gamma'_s=\rho_s\left[\frac{1}{B}\frac{dV_{ads}}{dp}+V_{ads}\frac{d}{dp}\left(\frac{1}{B}\right)\right], \tag{17}$$

being that we used the term source to represent the well flow through an internal boundary condition for the well-reservoir coupling:

$$q_{sc}=-J_w\left(p-p_{wf}\right), \tag{18}$$

where J_w is the productivity index, and p_{wf} is the pressure in the well [14]. In this work, we employ a prescribed production flow condition.

We know that Eq. (15) is a partial nonlinear parabolic differential equation that we use to determine the gas pressure. As an initial condition, we consider

$$p(x,y,t=0)=p_{ini}(x,y), \tag{19}$$

where p_{ini} is the initial pressure before the reservoir is disturbed by production/injection.

On the other hand, the external boundary conditions are those of null flow at the borders

$$\left(\frac{\partial p}{\partial x}\right)_{x=0,L_x}=\left(\frac{\partial p}{\partial y}\right)_{y=0,L_y}=0, \tag{20}$$

where L_x and L_y are the respective lengths of the reservoir in the x- and y- directions.

III. NUMERICAL METHODOLOGY

In this work, we use the Finite Difference Method (FDM) and a computational mesh of centered blocks [2, 14], together with a well-reservoir coupling technique [10], to determine the pressures in the reservoir and the producing well.

3.1. Discretization of the governing equation

We provide a schematic representation of a discretized two-dimensional domain is provided considering a single cell in the direction of the z-axis (highlighted in Fig. 2). We obtain the numerical solution at the nodes of the computational mesh, located in the centers of the cells. n_x and n_y represent the number of cells in the x- and y- directions, respectively. The integer indexes i and j represent the numbering of the cell nodes in the respective x- and y- directions, and the fractional indexes $i\pm1/2$ and $j\pm1/2$ their interfaces.

Therefore, by writing the governing equation as being evaluated in cell node i,j, and at time level $n+1$:

https://dx.doi.org/10.22161/ijaers.711.14 ISSN: 2349-6495(P) | 2456-1908(O)

$$\left[\frac{\partial}{\partial x}\left(\mathbb{T}'_x\frac{\partial p}{\partial x}\right)dx+\frac{\partial}{\partial y}\left(\mathbb{T}'_y\frac{\partial p}{\partial y}\right)dy\right]_{i,j}^{n+1}$$

$$=\left[\left(\Gamma_p+\Gamma_s\right)\frac{\partial p}{\partial t}+q_{sc}\right]_{i,j}^{n+1}, \tag{21}$$

where, as $V_b = dxdyL_z$, we used

$$\left(V_b\right)_{i,j}=\left(\Delta x\Delta y\right)_{i,j}L_z \tag{22}$$

and we introduced the variables

$$\mathbb{T}'_x\equiv\frac{A_xk_{a,x}}{\mu B} \tag{23}$$

and

$$\mathbb{T}'_y\equiv\frac{A_yk_{a,y}}{\mu B}, \tag{24}$$

with $A_x = \Delta yL_z$ and $A_y = \Delta xL_z$. $\Delta x_{i,j}$ and $\Delta y_{i,j}$ are, respectively, the mesh spacing in the x- and y-directions in the cell (i, j), and L_z the length of the rock formation in the z-direction.

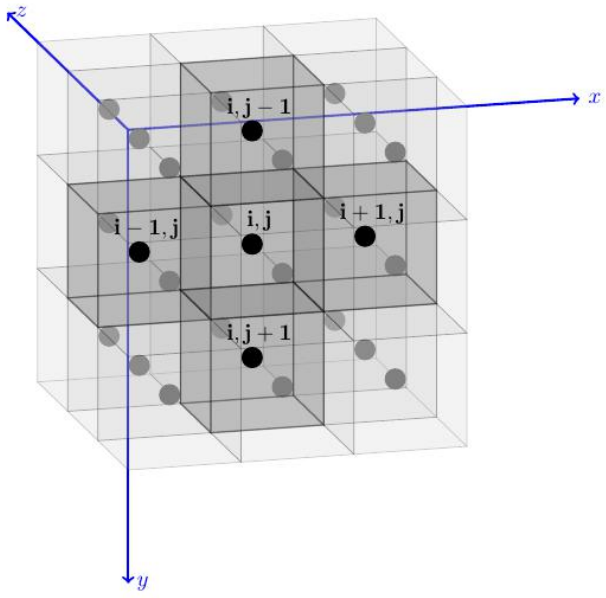

Fig. 2: *Example of some cells of the discretized domain.*

Then, we employ a centered difference type scheme to approximate the spatial derivative in the x-direction [2, 14],

$$\frac{\partial}{\partial x}\left(\mathbb{T}'_x\frac{\partial p}{\partial x}\right)_{i,j}^{n+1}\cong\frac{1}{\Delta x_{i,j}}\left[\left(\mathbb{T}'_x\frac{\partial p}{\partial x}\right)_{i+\frac{1}{2},j}\right]^{n+1}$$

$$-\frac{1}{\Delta x_{i,j}}\left[\left(\mathbb{T}'_x\frac{\partial p}{\partial x}\right)_{i-\frac{1}{2},j}\right]^{n+1}. \tag{25}$$

Spatial derivatives, evaluated on the faces of cells, are also discretized by centered differences,

$$\left(\frac{\partial p}{\partial x}\right)_{i+\frac{1}{2},j}^{n+1}\cong\frac{p_{i+1,j}^{n+1}-p_{i,j}^{n+1}}{\Delta x_{i+\frac{1}{2},j}} \tag{26}$$

and

$$\left(\frac{\partial p}{\partial x}\right)_{i-\frac{1}{2},j}^{n+1}\cong\frac{p_{i,j}^{n+1}-p_{i-1,j}^{n+1}}{\Delta x_{i-\frac{1}{2},j}} \tag{27}$$

where $\Delta x_{i\pm1/2,j}$ is the distance between the centers of cells (i, j) and $(i \pm 1, j)$. We can obtain the approximations for derivatives in the y-direction in an analogous way.

We also introduced transmissibilities in the x- and y- directions:

$$\mathbb{T}_{x,i\pm\frac{1}{2},j}^{n+1}=\left(\frac{A_xk_{a,x}}{\mu B\Delta x}\right)_{i\pm\frac{1}{2},j}^{n+1} \tag{28}$$

and

$$\mathbb{T}_{y,i,j\pm\frac{1}{2}}^{n+1}=\left(\frac{A_yk_{a,y}}{\mu B\Delta y}\right)_{i,j\pm\frac{1}{2}}^{n+1} \tag{29}$$

where a harmonic mean is used to determine the values of areas and permeabilities in positions $(i\pm1/2, j)$ and $(i, j \pm 1/2)$, from the values known in neighboring nodes. With regard to the properties of the fluid, we applied an arithmetic mean [14].

Thus, using an Euler approximation for the time derivative and a fully implicit formulation in time, it is possible to obtain the final discretized form of Eq. (21),

https://dx.doi.org/10.22161/ijaers.711.14 ISSN: 2349-6495(P) | 2456-1908(O)

$$\mathbb{T}_x\Big|_{i+1/2,j}^{n+1}\left(p_{i+1,j}^{n+1}-p_{i,j}^{n+1}\right)-\mathbb{T}_x\Big|_{i-1/2,j}^{n+1}\left(p_{i,j}^{n+1}-p_{i-1,j}^{n+1}\right)$$

$$+\mathbb{T}_y\Big|_{i,j+1/2}^{n+1}\left(p_{i,j+1}^{n+1}-p_{i,j}^{n+1}\right)-\mathbb{T}_y\Big|_{i,j-1/2}^{n+1}\left(p_{i,j}^{n+1}-p_{i,j-1}^{n+1}\right)$$

$$=\left(\frac{\Gamma_p+\Gamma_s}{\Delta t}\right)_{i,j}^{n+1}\left(p_{i,j}^{n+1}-p_{i,j}^{n}\right)+\left(q_{sc}\right)_{i,j}^{n+1} \tag{30}$$

where n indicates the time level at which we know the pressure, and we used a conservative expansion for the accumulation term [14]:

$$\Gamma_p^{n+1}=V_{bi,j}\left[\frac{c_\phi\phi^0}{B^n}+\phi^{n+1}\frac{d}{dp}\left(\frac{1}{B}\right)\right]_{i,j} \tag{31}$$

and

$$\Gamma_s^{n+1}=V_{bi,j}\left[\rho_s V_{ads}^n\frac{d}{dp}\left(\frac{1}{B}\right)+\frac{\rho_s}{B^{n+1}}\frac{dV_{ads}}{dp}\right]_{i,j}. \tag{32}$$

3.2. Well-reservoir coupling

We proceed with the process of discretization and the source term $(q_{sc})_{i,j}^{n+1}$ takes the discrete form

$$\left(q_{sc}\right)_{i,j}^{n+1}=-\left(J_w\right)_{i,j}^{n+1}\left[p_{i,j}^{n+1}-\left(p_{wf}\right)_{i,j}^{n+1}\right], \tag{33}$$

and the productivity index is expressed by [24]

$$\left(J_w\right)_{i,j}^{n+1}=\left[\frac{2\pi L_z\sqrt{k_{a,x}k_{a,y}}}{B\mu\,\ln\left(\frac{r_{eq}}{r_w}\right)}\right]_{i,j}^{n+1} \tag{34}$$

where r_w is the radius of the well and the equivalent radius, r_{eq}, is given by [24]

$$r_{eq_{i,j}}=\frac{0,28\left(\sqrt{\sqrt{\frac{k_{a,y}}{k_{a,x}}}\Delta x^2+\sqrt{\frac{k_{a,x}}{k_{a,y}}}\Delta y^2}\right)_{i,j}}{\left(\sqrt[4]{\frac{k_{a,y}}{k_{a,x}}}+\sqrt[4]{\frac{k_{a,x}}{k_{a,y}}}\right)_{i,j}} \tag{35}$$

and we already rewrote the equivalent radius for its use with the apparent permeability.

3.3. Linearization

Equation (30) forms a system of nonlinear algebraic equations [17]. From Eq. (33), for the particular case of the two-dimensional problem, we can isolate the pressure of the vertical well once we know the flow and the pressure of the reservoir at the end of each time step.

To achieve the linearization of Eq. (30), we adopted the well-known method of Picard [22]. Therefore, after its linearization, we get the following equation

$$\mathbb{T}_y\Big|_{i,j-1/2}^{v,n+1}p_{i,j-1}^{v+1,n+1}+\mathbb{T}_x\Big|_{i-1/2,j}^{v,n+1}p_{i-1,j}^{v+1,n+1}$$

$$+\mathbb{T}_x\Big|_{i+1/2,j}^{v,n+1}p_{i+1,j}^{v+1,n+1}+\mathbb{T}_y\Big|_{i,j+1/2}^{v,n+1}p_{i,j+1}^{v+1,n+1}$$

$$-\left[\mathbb{T}_y\Big|_{i,j-1/2}^{v,n+1}+\mathbb{T}_x\Big|_{i-1/2,j}^{v,n+1}+\left(\frac{\Gamma_p+\Gamma_s}{\Delta t}\right)_{i,j}^{v,n+1}\right]p_{i,j}^{v+1,n+1}$$

$$-\left[\mathbb{T}_x\Big|_{i+1/2,j}^{v,n+1}+\mathbb{T}_y\Big|_{i,j+1/2}^{v,n+1}\right]p_{i,j}^{v+1,n+1}$$

$$=\left(q_{sc}\right)_{i,j}^{v,n+1}-\left(\frac{\Gamma_p+\Gamma_s}{\Delta t}\right)_{i,j}^{v,n+1}p_{i,j}^{n} \tag{36}$$

and transmissibilities, Γ_p, Γ_s, and q_{sc} are evaluated at the iterative level v.

Then, we utilize the values determined at the iterative level v to calculate the pressure at $v+1, n+1$. Therefore, we obtain the pressure from two internal and external iterative processes for a given time step [8].

We choose the method of the Conjugate Gradient (CG) to solve the algebraic system of Eq. (36) [16, 25].

We can find in Fig. 3 the flowchart of the numerical scheme of the resolution algorithm for a single time step calculation. To verify whether we achieve the convergence of the internal and external iterations, we use tolerance values equal to tol_1 and tol_2, respectively.

IV. RESULTS

In this section, we present our numerical results. Initially, we introduce the standard case and some information about the data used in the simulations, in-

https://dx.doi.org/10.22161/ijaers.711.14 ISSN: 2349-6495(P) | 2456-1908(O)

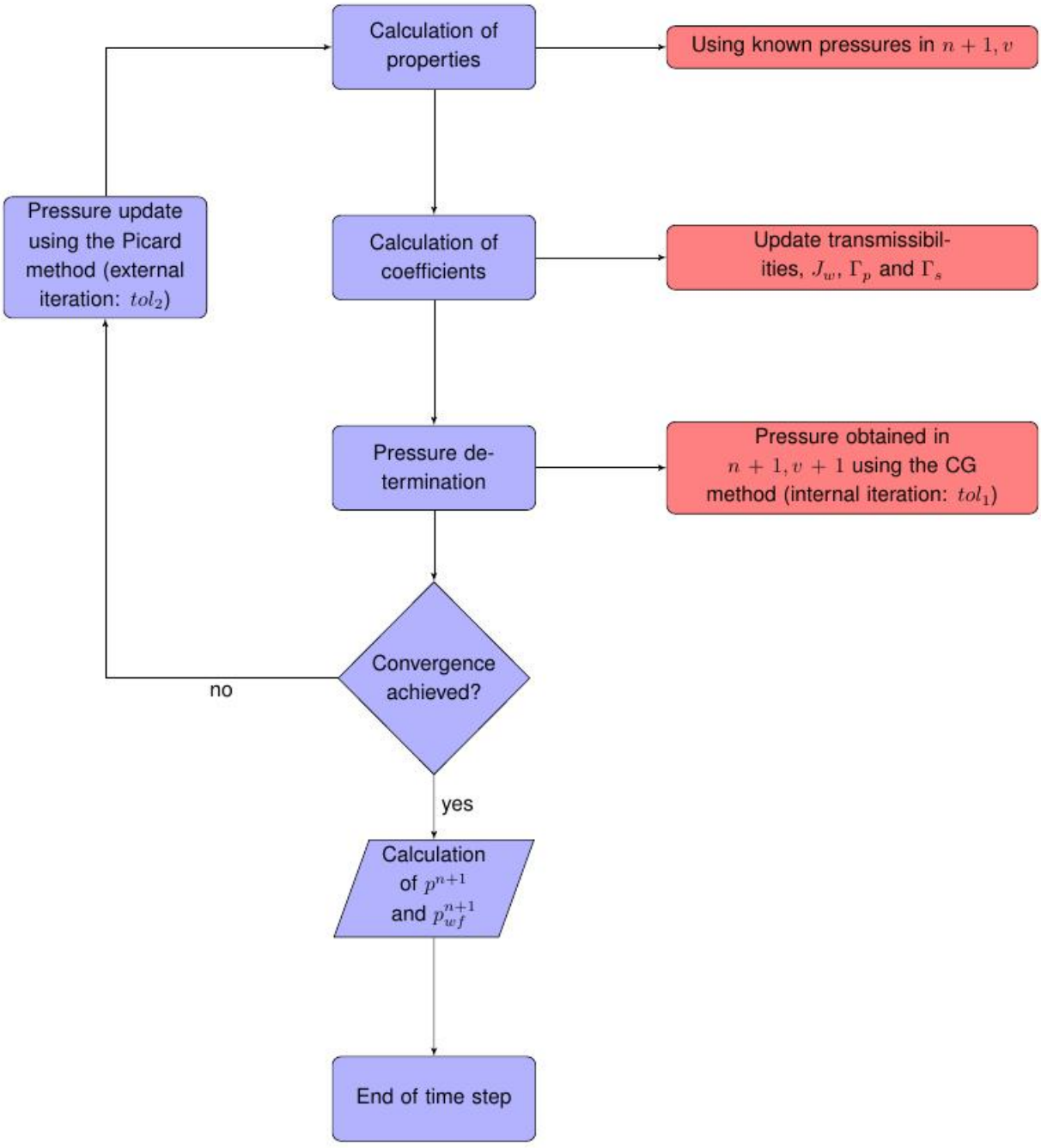

Fig. 3: *Flowchart for a single time step.*

https://dx.doi.org/10.22161/ijaers.711.14 ISSN: 2349-6495(P) | 2456-1908(O)

cluding rock and fluid properties, simulation parameters, and geometric data.

Next, we do a numerical verification study, including the refinement of the computational mesh. Finally, we carry out a sensitivity study of parameters and compare the different models employed. Here, the standard model is that incorporating the effects of gas slippage and adsorption in the modified Darcy's law, as discussed in Jiang and Younis [18].

We show the results using specialized plots, commonly employed in the area of well pressure test analysis [5].

We consider six models according to how we calculate the apparent permeability values ($\mathbf{k}_a$) in Eq. (1) and the Γ_s coefficient in Eq. (15):

- Model 1 [14], which represents the classic case of Darcy's law, without the effects of slippage and adsorption;
- Model 2 [15], the apparent permeability is calculated as a function of the Knudsen number (slippage effect);
- Model 3 [3], without slippage effect and with an accumulation term for the inclusion of adsorption;
- Model 4 [21], apparent permeability corrected as a function of the Knudsen number (slippage effect) and insertion of adsorption through the source term in Eq. (15);
- Model 5, we modify the apparent permeability taking into account adsorption and, also, we introduce its effects via the accumulation term in Eq. (15);
- Model 6 [18], we change the value of $\mathbf{k}_a$ to take into account the combined effects of slippage and adsorption, and we also include the term $\Gamma_s \neq 0$ in Eq. (15).

We modify the initial time step (Δt_{ini}) according to the growth rate ($\delta_{\Delta t}$) to obtain the next time step. This procedure is interrupted when we reach the specified final time step (Δt_{max}). We employ this strategy to achieve greater accuracy in the initial stages of production.

We can find the default values used in the simulations in Table 1. They are defined based on the works of [21], [18] and [9]. We adopt the same tolerance value for the internal (tol_1) and external (tol_2) iterative procedures.

Table 1: *Parameters for the default case.*

Parameter	Value	Unit
c_ϕ	1.0×10^{-6}	psi^{-1}
d_m	2.3×10^{-10}	ft
$k_x = k_y$	5.0×10^{-6}	Darcy
$L_x = L_y$	4,000	ft
L_z	40.0	ft
L_{wf}	40.0	ft
$n_x = n_y$	321	–
p_{sc}	14.65	psi
p_L	1,100	psi
$p_{ini} = p^0$	6,000	psi
Q_{sc}	-5.0×10^4	scf/day
r_w	0.25	ft
R	10.73	ft^{3}psi/R lbm-mol
t_{max}	365	day
$tol_1 = tol_2$	1.0×10^{-4}	psi
T	609.67	R
T_{sc}	519.67	R
V_L	0.0005	ft^3/lbm
γ	0.6	psi
$\delta_{\Delta t}$	1.05	–
Δt_{ini}	0.01	day
Δt_{max}	10.0	day
ρ_s	200.0	lbm/ft^3
τ	1.41	–
$\phi_{ini} = \phi^0$	0.12	–

We use the relative density of the gas, together with the pressure and temperature values, to determine the other properties of the gas [8, 20, 26].

4.1. Mesh refinement

Table 2 shows the numbers of cells used in the generation of the different computational meshes applied in the study of refinement of the computational mesh.

As the production time increases, we can see (Fig. 4) that the pressure curves of the well approach each other. However, for the initial instants of time, there is no overlap of values due to the increased effect of the well known numeric artifact [10, 11].

https://dx.doi.org/10.22161/ijaers.711.14 *ISSN: 2349-6495(P) | 2456-1908(O)*

The numerical artifact appears as a consequence of the well-reservoir coupling technique, that assumes a steady-state flow regime near the well [23, 24]. Nevertheless, its effects do not compromise the results for the advanced time instants. So, having verified the numerical convergence, Mesh 5 was chosen as the standard, given the significant reduction of the numerical artifact for times higher than one day of production.

Table 2: *Meshes.*

Mesh	n_x	n_y
1	21	21
2	41	41
3	81	81
4	161	161
5	321	321
6	641	641

We emphasize that de Souza [9] validated the simulator used in the present work by comparing its results with those of the commercial simulator IMEX [6] for Model 1.

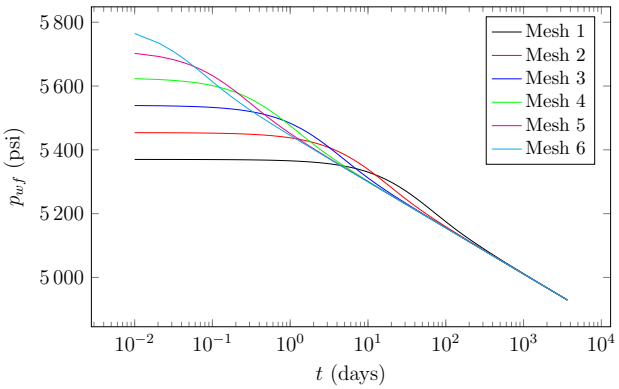

Fig. 4: *Results for mesh refinement.*

4.2. Sensitivity analysis and model comparison

After conducting the mesh refinement study, we performed a sensitivity analysis considering the different models for the single-phase flow of natural gas, incorporating (or not) the slippage and gas adsorption phenomena. We must remark that for all the studied cases, the Kn remained within the validity range of the slip flow regime [4].

Initially, we compare the results obtained with Models 1 (Fig. 5) and 6 (Fig. 6) in simulations by varying the absolute permeability. We can see in Fig. 5 that for the highest values of absolute permeability, there are the smallest pressure variations in the well. In the graphs, the sloping lines are characteristic of the transient regime in a porous medium. In Fig. 6, again, for the highest permeabilities, there is the smallest pressure variation in the well. We also observed the occurrence of the transient regime. However, compared with Fig. 5, it appears that the results for Model 6 show a lower pressure drop than those for Model 1, for the same absolute permeability, as a result of higher apparent permeability. It also leads to a shorter duration and magnitude of the numerical artifact. Besides that, we should note that a lower absolute permeability leads to a higher Kn [8], thus leading to a lower pressure drop, in contrast to the effect of the absolute permeability in the modified Darcy's law.

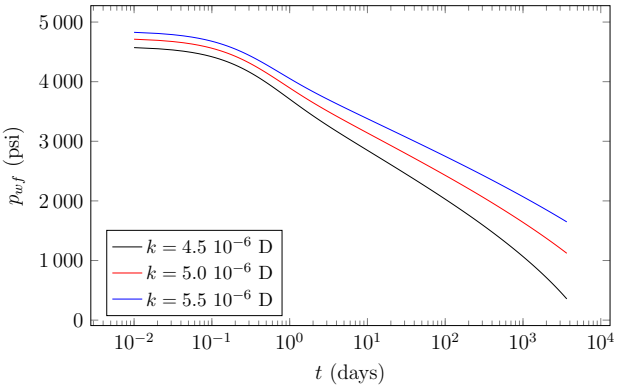

Fig. 5: *Permeability variation for Model 1.*

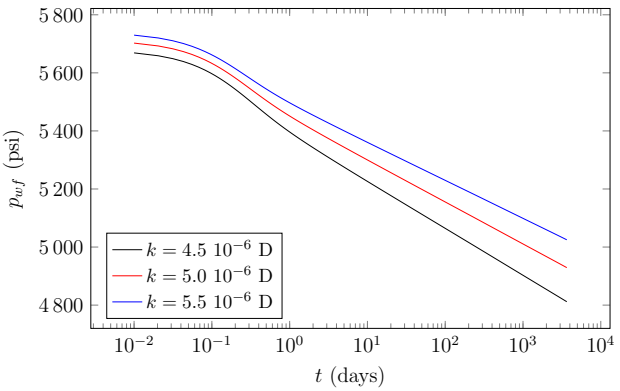

Fig. 6: *Permeability variation for Model 6.*

About temperature variation for Model 6, see Fig. 7, its increase leads to an augmentation in the Knudsen number (via λ) and, consequently, to a

https://dx.doi.org/10.22161/ijaers.711.14 ISSN: 2349-6495(P) | 2456-1908(O)

growth in the permeability apparent (facilitating the flow), which contributes to a lower pressure drop. However, the viscosity of the gas rises with temperature too. Thus, it also causes an increase in pressure drop due to the higher resistance to flow. Therefore, there is a contraposition of effects that leads to different trends about pressure variation, with growth in pressure drop for increasing temperature being prevalent in the tested cases.

We can see in Fig. 8 the influence that V_L has on the term source (due to adsorption) and the apparent permeability. We noticed that the curves are close in the initial moments and that at a later time, there is a gap between them. For the higher volume of Langmuir, there is a higher amount of adsorbed gas that can be released, favoring the maintenance of production (less pressure drop). We know that the increase of V_L causes a reduction in the apparent permeability. However, with the release of the adsorbed gas, the effect of V_L on $\mathbf{k'}_a$ decreases.

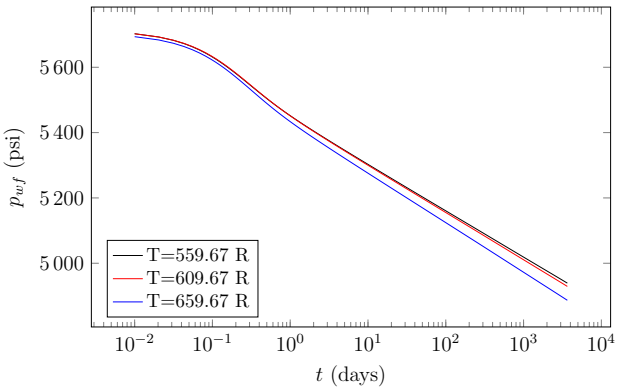

Fig. 7: *Temperature variation for Model 6.*

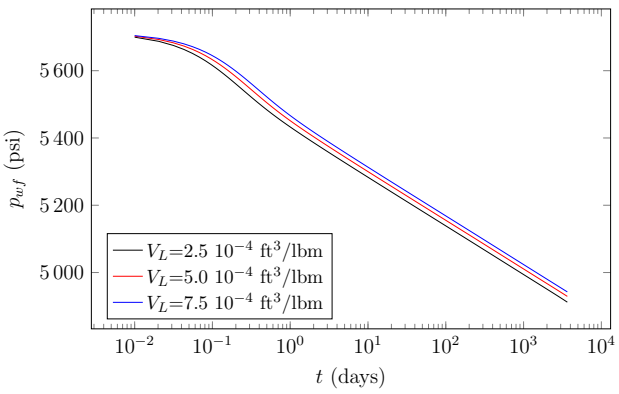

Fig. 8: *Variation of V_L for Model 6.*

In the last case studied, we compare the six flow models, and we show the results in Fig. 9. Indeed, we should point out that we have not found Model 5, $\mathbf{k}_a = \mathbf{k'}_a$ and $\Gamma_s \neq 0$, in the literature. Nevertheless, it could be used, for example, in reservoir simulations where the effects of adsorption are considerable, although we can neglect those of slippage.

When comparing Models 1 and 2, we observe that the incorporation of the slippage effect leads to a lower pressure drop due to the higher values of apparent permeability. The curves start from different points and have different slopes, in the region of the transient flow, due to the difference in apparent permeabilities. In the specific case of Models 1 and 3, the curves begin close with each other, as the apparent permeabilities are the same (the absolute). Further, we observe that the slopes are similar in the region of the transient regime (except for the effects of non-linearities) due to the properties of the fluid, with a lower pressure drop for the case where adsorption supplements production.

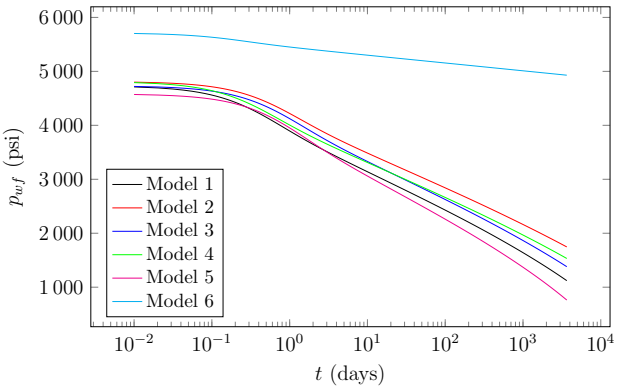

Fig. 9: *Comparison between different models.*

For Models 1 and 4, we perceive that adsorption and slippage effects favor the maintenance of pressure. Because of the slippage effect, we must correct the permeability apparent. As a consequence, the slope of these curves is not similar to those of Models 1 and 3. Indeed, they are closer to that of Model 2. However, the overlapping effects of slippage and adsorption did not lead to values of pressure higher than those obtained in Model 2. We can explain this behavior by the fact that Kn depends on pressure so that for higher pressure values, there is a decrease in Kn and a higher resistance to flow. In the case of Model 3, the overlapping effects lead to higher pres-

https://dx.doi.org/10.22161/ijaers.711.14 ISSN: 2349-6495(P) | 2456-1908(O)

sure values after about 20 days of production.

As the apparent permeability in Model 5 is lower than the absolute permeability, at least at the beginning of production, the numerical artifact appears more strongly. In the beginning, the production potential is lower, but over time the increase in Langmuir volume results in a higher amount of adsorbed gas that can be released, favoring the maintenance of production (less pressure drop). Even so, this situation is transient, and Model 1 has a lower pressure drop over long periods. A possible explanation is associated with the pressure variation in the reservoir since it has a limited direct impact on $\mathbf{k}_a$ and because the model only considers its correction based on V_L. Therefore, the predominant effect becomes that of the accumulation term, and lower pressure drops than those of Model 1 would only be possible for even higher values of V_L.

Finally, for Model 6, the difference in pressure drop is highlighted when slippage and adsorption phenomena are not neglected, as in the case of Model 1. Although the effects are opposite concerning the variation in apparent permeability (predominant in the cases studied here), adsorption contributes to sustaining production through the accumulation term.

V. CONCLUSION

As expected, we showed the positive influence of adsorption once we have more gas available for production as a consequence of this phenomenon, despite its negative impact on the calculation of the apparent permeability. On the other hand, we also remarked the benefits of the slippage effect on increasing the apparent permeability, facilitating flow through the reservoir. Besides, we were able to capture the influence of non-Darcy models in the well-reservoir coupling by analyzing the pressure variation of the producing well during production.

Therefore, it was clear, given the results obtained, that for single-phase gas flow in shale-type reservoirs, failure to consider both phenomena of slippage and gas adsorption may result in incorrect values for pressures in the well and the gas reservoir. Such a fact may lead to mistaken decision making. For example, we can invest resources in the production of a deposit that will present less pressure on the producing well than expected or failing to invest in a reservoir that would have favorable production conditions. As we have seen, this can happen if we do not consider these two effects. Further, we could perform simulations resulting in production flows closer to real conditions if we take into account both slippage and adsorption phenomena.

In the case of shale gas reservoirs, due to their characteristics, we must not forget that their feasibility is possible through the use of horizontal producing wells and hydraulic fracturing.

REFERENCES

[1] Ali, W. (2012). Modeling gas production from shales and coal-beds. Master's thesis, Stanford University.

[2] Aziz, M. and Settari, A. (1990). *Petroleum Reservoir Simulation*. Elsevier Applied Science, New York, USA.

[3] Berawala, D. S. (2015). Modeling of gas production from tight shale formations: an innovative approach. Master's thesis, University of Stavanger, Stavanger, Norway.

[4] Bestok, A. e Karniadakis, G. E. (1999). A model for flows in channels, pipes, ans ducts at micro and nano scales. *Microscale Thermophysical Engineering*, 3:43–77.

[5] Bourdet, D. (2002). *Well Test Analysis: the Use of Advanced Interpretation Models*. Handbook of Petroleum Exploration and Production 3. Elsevier, Amsterdam.

[6] CMG (2009). *IMEX, Advanced Oil/Gas Reservoir Simulator*. Computational Modeling Group.

[7] Darcy, H. (1856). *Les fontaines publiques de la ville de Dijon : exposition et application des principes à suivre et des formules à employer dans les questions de distribution d'eau*. Victor Dalmont, Paris, France.

[8] de Oliveira, M. L. (2018). Estudo comparativo de modelos não–Darcy para *shale gas*. Instituto Politécnico, Universidade do Estado do Rio de Janeiro. Undergraduate project. In Portuguese.

[9] de Souza, G. (2013). *Acoplamento Poço-reservatório na Simulação Numérica de Reservatórios de Gás*. PhD thesis, Universidade Estadual do Norte Fluminense, Macaé, Brasil. In Portuguese.

https://dx.doi.org/10.22161/ijaers.711.14 ISSN: 2349-6495(P) | 2456-1908(O)

[10] do Rosário, R. C. D., de Souza, G., and Amaral Souto, H. P. (2020). A comparative study of some well-reservoir coupling models in the numerical simulation of oil reservoirs. *International Journal of Advanced Engineering Research and Science*, 7(9):126–148.

[11] Dumkwu, F., Akand, I., and Carlson, E. S. (2012). Review of well models and assessment of their impacts on numerical reservoir simulation performance. *Journal of Petroleum Science and Engineering*, 82–83:174–186.

[12] Economides, M. J. and Wood, D. A. (2009). The state of natural gas. *Journal of Natural Gas Science and Engineering*, 16:1–4.

[13] EPE (2020). Balanço energético nacional. Technical report, Empresa de Pesquisa Energética, Ministério de Minas e Energia, Brasília, DF, Brazil. In Portuguese.

[14] Ertekin, T., Abou-Kassem, J. H., and King, G. R. (2001). *Basic Applied Reservoir Simulation*. SPE Textbook Series 7. Society of Petroleum Engineers, Richardson.

[15] Florence, F. A., Rushing, J. A., Newsham, K. E., and Blasingame, T. A. (2007). Improved permeability prediction relations for low permeability sands. In *Society of Petroleum Engineers Rock Mountain Oil & Gas Technology Symposium*, Denver, Colorado, USA.

[16] Hestenes, M. R. and Stiefel, E. (1952). Method of conjugate gradients for solving linear systems. *Journal of Research of the National Bureau Standards*, 49(6):409–436.

[17] Islam, M. R., Moussavizadegan, S. H., Mustafiz, S., and Abou-Kassem, J. H. (2010). *Advanced Petroleum Reservoir Simulation*. Scrivener Publishing LLC., Salem, USA, 1 edition.

[18] Jiang, J. and Younis, R. M. (2015). A multimechanistic multicontinuum model for simulating shale gas reservoir with complex fractured system. *Fuel*, 161:333–344.

[19] Klinkenberg, L. J. (1941). The permeability of porous media to liquids and gases. *Drilling and Production Practice, American Petroleum Inst.*, pages 200–213.

[20] Lee, A., Gonzalez, M., and Eakin, B. (1966). The viscosity of natural gases. *Journal of Petroleum Technology, Transactions of AIME*, 18:997–1000.

[21] Li, D., Zhang, L., Wang, J. Y., Lu, D., and Du, J. (2016). Effect of adsorption and permeability correction on transient pressures in organic rich gas reservoirs: Vertical and hydraulically fractured horizontal wells. *Journal of Natural Gas Science and Engineering*, 31:214–225.

[22] Nick, H. M., Raoof, A., Centler, F., Thullner, M., and Regnier, P. (2013). Reactive dispersive contaminant transport in coastal aquifers: Numerical simulation of a reactive Henry problem. *Journal of Contaminant Hydrology*, 145:90–104.

[23] Peaceman, D. W. (1978). Interpretation of well-block pressures in numerical reservoir simulation. *Society of Petroleum Engineers Journal*, 18(3):183–194.

[24] Peaceman, D. W. (1983). Interpretation of well-block pressures in numerical reservoir simulation with nonsquare grid blocks and anisotropic permeability. *Society of Petroleum Engineers Journal*, 23(3):531–543.

[25] Saad, Y. (2003). *Iterative Methods for Sparse Linear Systems*. Society of Industrial and Applied Mathematics, USA, 2 edition.

[26] Sanjari, E. and Lay, E. N. (2011). An accurate empirical correlation for predicting natural gas compressibility factors. *Journal of Natural Gas Chemistry*, 21:184–188.

[27] Wang, C. (2013). Pressure transient analysis of fractured wells in shale reservoirs. Master's thesis, Colorado School of Mines, Colorado, USA.

[28] Wang, L., Tian, Y., Wang, C., Yao, B., Wang, S., Winterfeld, P. H., Wang, X., Yang, Z., Wang, Y., Cui, J., and Wu, S. (2017). Advances in improved/enhanced oil recovery technologies for tight and shale reservoirs. *Fuel*, 210:425–445.

[29] Wang, X. (2009). The state of the art in natural gas production. *Journal of Natural Gas Science and Engineering*, 1(1):14–24.

[30] Yu, W. and Sepehrnoori, K. (2014). Simulation of gas desorption and geomechanics effects for unconventional gas reservoirs. *Fuel*, 116:455–464.

https://dx.doi.org/10.22161/ijaers.711.14 *ISSN: 2349-6495(P) | 2456-1908(O)*

[31] Zárante, P. and Sodré, J. (2009). Evaluating carbon emissions reduction by use of natural gas as engine fuel. *Journal of Natural Gas Science and Engineering*, 1(6):216–220.